Results in Surfaces and Interfaces 20 (2025) 100558

Contents lists available at ScienceDirect

Results in Surfaces and Interfaces

journal homepage: www.elsevier.com/locate/rsurfi

Development and characterization of biopolymer-hydroxyapatite composites for efficient lead removal

Maria M. Espinola Colmán *, Lucas Medina, Pablo Casanova, Maria B. Martinez P, Magna Monteiro

Bio & Materials Laboratory, Polytechnic School, National University of Asuncion, San Lorenzo, Paraguay

ARTICLE INFO

Keywords:
Lead
Bioadsorption
Sodium alginate
Biological agar
Hydroxyapatite
Noodles
Beads

ABSTRACT

Heavy metals in wastewater require special attention due to their toxic effects on humans. The removal of these metals can be costly and challenging. Biosorption is an alternative removal method using biological materials with metal-sequestering properties. This study investigates the biosorption process using sodium alginate (SA), biological agar (BA), and hydroxyapatite (Hap) in two different shapes: beads and noodles. The Hap/SA/BA solution was added into a $CaCl_2$ solution, forming a Hap/SA/BA composite through coagulation. The adsorbents were characterized using Fourier-transform infrared spectroscopy (FTIR), X-ray diffraction (XRD), and scanning electron microscope (SEM) coupled with energy-dispersive X-ray spectroscopy (EDS). Atomic absorption analysis was performed to determine the residual lead concentrations. The results indicated that the adsorption process for all samples fitted the pseudo-second-order kinetic model. The maximum sorption capacity of the sample was 98.5 mg of Pb^{2+}/g. Noodle-shaped samples exhibited faster adsorption kinetics than bead-shaped ones; however, the final amount of Pb^{2+} removed was nearly identical across all samples. This study provides valuable evidence for the ongoing development of different shapes of ceramic/polymer composites for environmental applications.

1. Introduction

Water is an essential element and vital requirement for all living beings; however, its availability has become a significant issue due to the increasing demand and the scarcity of pure water sources [1]. This problem is aggravated by industrial activities that produce and discharge large quantities of hazardous compounds into aquatic environments [2]. Contamination of water bodies due to heavy metals, such as lead, must receive special attention due to the toxic effects these substances can have on humans.

Lead is a ductile element that is easily extracted, making it one of the first heavy metals discovered and used by humans [3]. However, this heavy metal cause various adverse health effects, such as increased blood pressure, cardiovascular disease, mental impairment, anemia, and decreased renal function [4]. Water contaminated with lead should be treated to protect the water source and ensure safe water supplies using various methods, as documented in several studies. Alternative methods for removing $Pb^{2}+$ from water include several techniques such as chemical precipitation, chemical oxidation or reduction, ion exchange, ion exchange, adsorption, filtration, membrane technologies, and evaporation recovery [5,6]. Among these methods, adsorption shows efficient results, lower cost, and environmental safety, and it has been used in industrial effluent treatments [7].

Bioadsorption is an alternative removal method based on metal-sequestering properties using biological materials as adsorbents [6,8]. Some of these materials include hydroxyapatite (Hap) ($Ca_{10}(PO_4)_6(OH)_2$), sodium alginate (SA), and bacteriological agar (BA). Hap is an inorganic material with high biocompatibility because it is a main constituent of human bones, and it shows sorption capacity due to its chemical composition and crystal structure [9–11]. Since Hap is typically obtained in powder form, a ceramic foam production technique may be necessary for specific applications. On the other hand, SA and BA are polysaccharides; SA is derived from brown marine algae, while BA is extracted from red algae. The components of brown algae are cellulose, alginic acid (which is composed of mannuronic and guluronic acids, M and G, distributed along the polymer backbone), the corresponding salts (sodium, potassium, magnesium, and calcium), and sulfated polysaccharides (J. [12]). Meanwhile, some studies have reported the usage of sodium alginate as a potential chelator due to its capacity for ion exchange between the functional groups present on the polymer

* Corresponding author.
E-mail address: magdaespinola@pol.una.py (M.M. Espinola Colmán).

https://doi.org/10.1016/j.rsurfi.2025.100558
Received 30 December 2024; Received in revised form 10 April 2025; Accepted 13 May 2025
Available online 19 May 2025

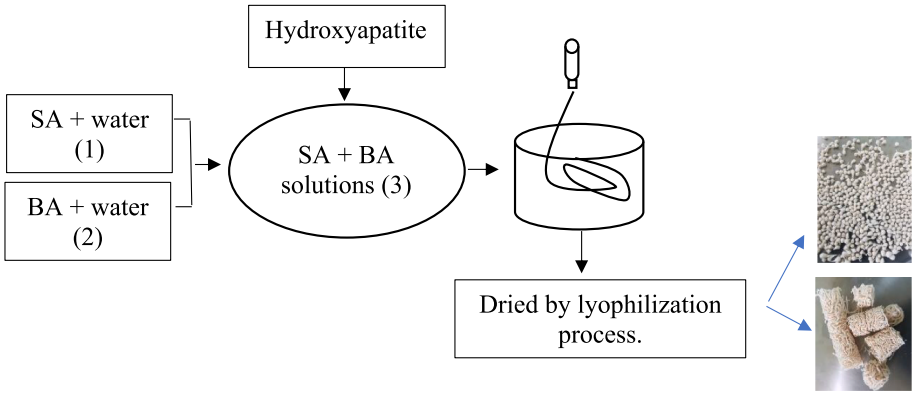

Fig. 1. Flowchart of the sodium-alginate-agar-based porous material production with hydroxyapatite (AAH).

backbone and the heavy metal ions (J. [12]), (B. [1,13]). Nevertheless, sodium alginate shows poor mechanical properties, such as high rigidity and fragility (B. [13]). In order to improve its mechanical properties, combining sodium alginate and another polymer could be necessary. Regarding red algae, most of it consists of microfibrils that provide rigidity and a mucilaginous matrix composed of galactose-based polymers (agar, funori, porphysan, and carrageenan), which provides a flexible behavior and slippery texture (J. [12]). The mentioned characteristics suggest the potential for developing a composite material since they are designed to enhance the functionality of a new material by taking advantage of the best properties of each component [14].

Many types of adsorbent composite materials have been studied. Googerdchian and collaborators introduced nanohydroxyapatite (nHap) into alginate polymer. Pure alginate film and nHap powder showed less capacity to adsorb lead than composite films ([15,16] investigated the adsorption performance of hydrogel beads made from graphene oxide/sodium alginate (GAD) in an aqueous manganese (II) solution. The GAD beads showed an attractive adsorption capacity of 56.49 mg/g [16].The sorption capacity of Hap-alginate/gelatin nanocomposite for lead and cadmium was investigated by Sangeetha and collaborators [17]. According to the results, the removal capacity of Hap-alginate/gelatin nanocomposite was 616 and 388 mg/g for lead and cadmium, respectively. Thus, it is possible to design and produce various types of materials suitable for metal decontamination in water.

This study aimed to evaluate the sorption capacity of a sodium alginate/biological agar/hydroxyapatite (AAH) composite as a filter for the heavy metal ion Pb^{2+}, utilizing two distinct porous structures: beads and noodles. The porous material was characterized by scanning electron microscopy (SEM) coupled with energy dispersive spectroscopy (EDS), Fourier-transform infrared spectroscopy (FTIR), and X-ray diffraction (XRD) to study its morphological and chemical structure. Atomic absorption was conducted to determine the residual concentration of lead in the solution.

2. Experimental

2.1. Materials

Sodium alginate was obtained from WillPowder (United States), and bacteriological agar was from Oxoid (England). Hydroxyapatite was developed by the GBioMat research group from bovine bone, with a particle size between 23 and 53 μm [18]. Anhydrous calcium chloride ($CaCl_2$), analytically pure, was purchased from Cicarelli (Argentina). Sorption analysis was conducted by dissolving lead nitrate ($Pb(NO_3)_2$) from Cicarelli (Argentina) in deionized water.

2.2. Methods

The production process of the AAH porous biocomposite was carried out as follows. Sodium alginate (SA) and bacteriological agar (BA) were dissolved separately in water using magnetic stirring, with a solution between 60 and 65 °C. Then, SA solution, BA solution, and hydroxyapatite were vigorously mixed using mechanical stirring for 1 h at 65 °C. A 10 mL syringe was used to add the homogenized mixture of SA and BA into a 2% anhydrous calcium chloride ($CaCl_2$) solution, forming "noodles" and "beads", respectively. After 40 min, the noodles or beads were removed and rinsed with distilled water. The porous material was then dried by lyophilization process for 24 h. Fig. 1 illustrates the process of biocomposite (sodium-alginate-agar) production.

Table 1 shows the recipes of the samples used in each experiment to produce porous materials under study. In Table 1, samples labeled AAH refer to the sodium alginate/biological agar/hydroxyapatite biocomposites, while samples labeled AA contain only biopolymers SA and BA. In addition, the letters B and N denote the bead and noodle formats of the filters, respectively.

Fig. 2 presents the two distinct forms of the synthesized AAH composite: beads and noodles.

2.3. Preparation of lead solution for sorption test

The removal of Pb^{2+} heavy metal was conducted in a batch process using five different adsorbents: the sodium alginate/biological agar/hydroxyapatite beads composite (AAH_B), the alginate/agar beads (AA_B), the alginate/agar/hydroxyapatite noodles composite (AAH_N), the alginate/agar noodles (AA_N), and pure hydroxyapatite (Hap). Before starting the test, the pH of a 100 mL lead solution, initially at 1000 mg/L concentration, was adjusted between 4.5 and 5, which represents the point of zero charge [1,18], by adding 0.1 N sodium hydroxide or 2.0 M chloridoid acid solutions. This adjustment was made to monitor the pH changes of the solution throughout the lead removal

Table 1
Recipes of the samples used as filters used in sorption tests for lead solution.

Samples	Sodium Alginate (g)	Agar (g)	Total mass of biopolymers (g)	Hap (g)	Total solid composition (g)	Distilled water (g)
AAH_B	2.4	0.8	3.2	1.6	4.8	520
AA_B	3.6	1.2	4.8	0	4.8	520
AAH_N	2.4	0.8	3.2	1.6	4.8	520
AA_N	3.6	1.2	4.8	0	4.8	520

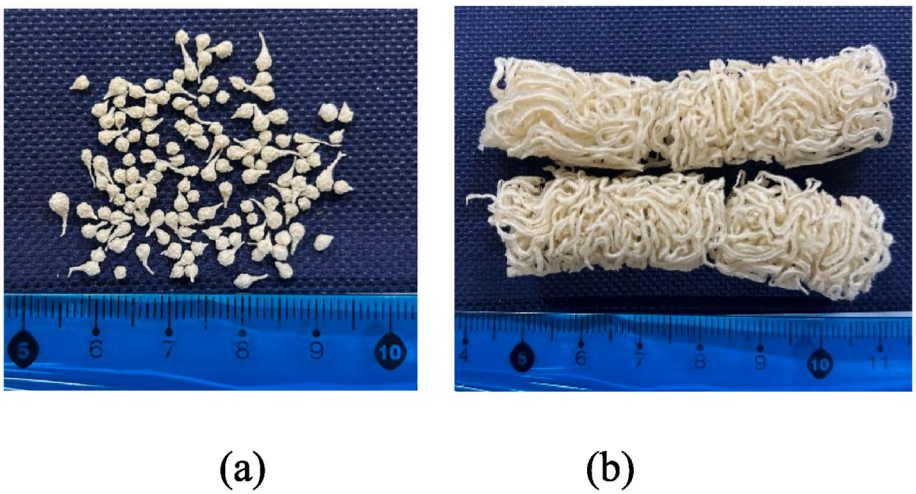

Fig. 2. Composites of sodium alginate/biological agar/hydroxyapatite (AAH) produced in this work in two forms: (a) beads; and (b) noodles.

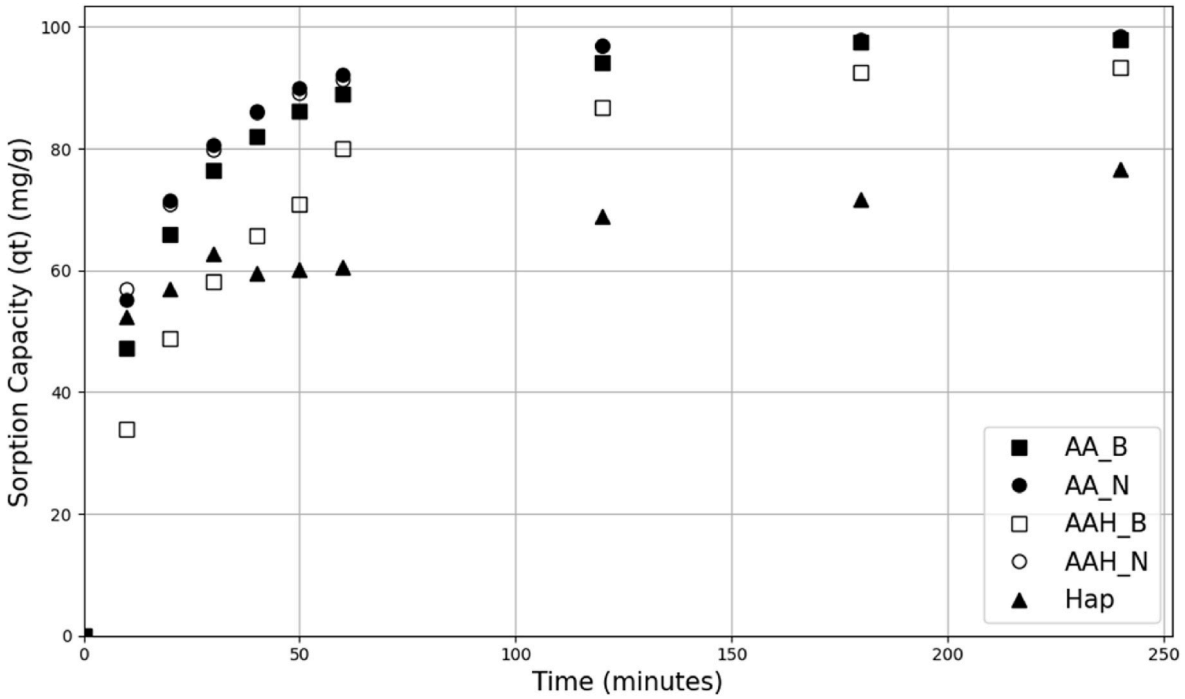

Fig. 3. Sorption capacity tests of Pb^{2+} ion removal of different adsorbents: AA_B, AA_N, AAH_B, AAH_N, and pure powder of Hap. Initial Pb^{2+} concentration:1000 mg/L; total contact time: 240 min; agitation speed: 250 rpm; adsorbent dosage: 1.0 g.

process. Then, 1.0 g of the desired adsorbent was added to the heavy metal solution at room temperature, using a magnetic stirrer at 250 rpm to shake the solution. Samples of the lead solution were collected at various times: 0, 10, 20, 30, 40, 50, 60, 120, 180 and 240 min. Later, the diluted solutions were analyzed by atomic absorption with a spectrophotometer (Thermo Scientific iCE 3000) to determine the remaining heavy metal concentration.

The amount of heavy metal concentration removed by the adsorbent, $q_{t,}$ was calculated using equation (1), and the removal efficiency was determined using equation (2):

$$q_t = \frac{(C_o - C_t)}{m_{absorbent}} V \quad (1)$$

$$\text{Removal efficiency } (\%) = \frac{(C_o - C_t)}{C_o} .100\% \quad (2)$$

Where C_o (g/l) is the initial heavy metal concentration, C_t (g/l) is the heavy metal concentration at a specific time, $m_{adsorbent}$ is the mass of the adsorbent (g), and V (l) is the volume of the solution. In addition, pseudo-first and pseudo-second-order models were applied to determine the best fit for the experimental data.

2.4. Characterization

The samples were dried through a 24-h lyophilization process and then coated with carbon using a rotary coater (Quorum, Model Q150R ES Plus) to study their morphology. Micrographs and chemical composition were obtained by SEM/EDS (ZEISS, Model EVO 15) with an accelerating voltage of 15 kV in a high vacuum. FTIR spectroscopy (Nicolet iS5, Thermo Fisher, USA) was performed using potassium bromide (KBr) pellets, with a resolution of 4 cm^{-1} in the range of

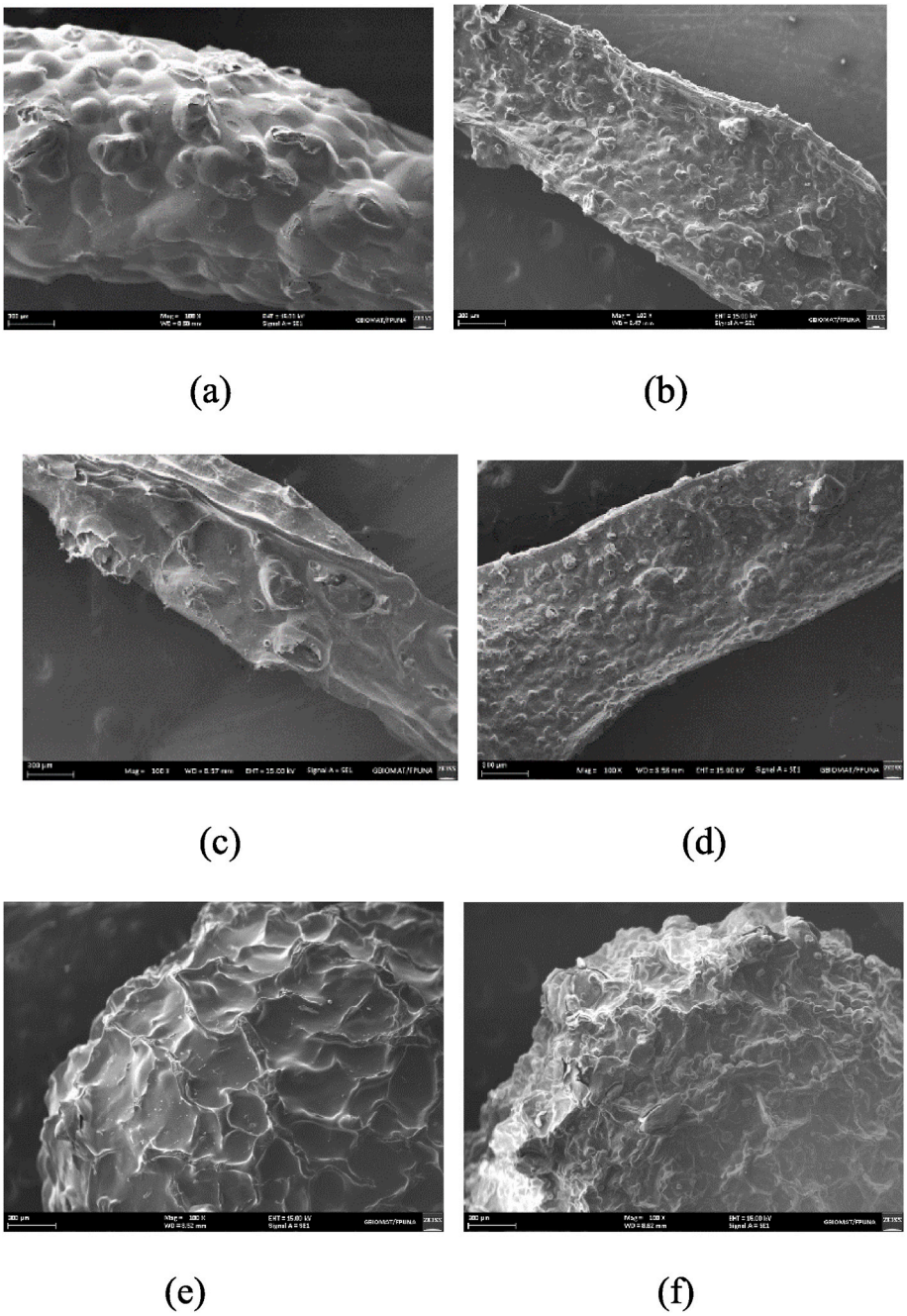

Fig. 4. SEM images of: AA_N and AAH_N samples before Pb^{2+} adsorption tests (a, b); AA_N and AAH_N samples after Pb^{2+} adsorption tests (c, d); AA_B and AAH_B samples before Pb^{2+}adsorption tests (e, f); AA_B and AAH_B samples after Pb^{2+}adsorption tests (g, h), (i) hydroxyapatite (Hap) used in the adsorption tests. Scale bar: 300 μm, magnification: 100X.

4000–400 cm^{-1} in transmission mode. XRD technique was conducted on a powder diffractometer (X'Pert3, Malvern PANalytical, Netherland), using Cuα radiation at an accelerating voltage of 40 kV, a current of 30 mA, 2θ angle range of 10–80°, scan step 0.02° and time step of 0.5 s.

3. Results and discussion

Fig. 3 shows Pb^{2+} adsorption process occurred within the first 50 min for all the samples. However, the adsorption rates for the noodles adsorbents, both with and without Hap, were slightly faster in the first 10 min than those for the bead samples. In addition, the data reveals that the adsorption capacity of Hap (powder) was lower. Googerdchian et al. [15] reported that the sorption capacity of pure nanohydroxyapatite was lower than that of pure alginate film after both samples were in contact with Pb^{2+} solution for 6 h. The authors also found that the composite film containing nanohydroxyapatite/alginate performed better in heavy metal uptake than composite beads. This is likely due to the larger surface area of the noodle adsorbents, which exhibited the highest initial adsorption rates [19].

The surface area and the porosity of the sodium alginate (SA)/biological agar/hydroxyapatite play an important role in the adsorption process; a larger surface area provides more active sites available for lead ions to attach, enhancing adsorption efficiency. In addition, the porosity increases exposure to lead, maximizing interaction, because the

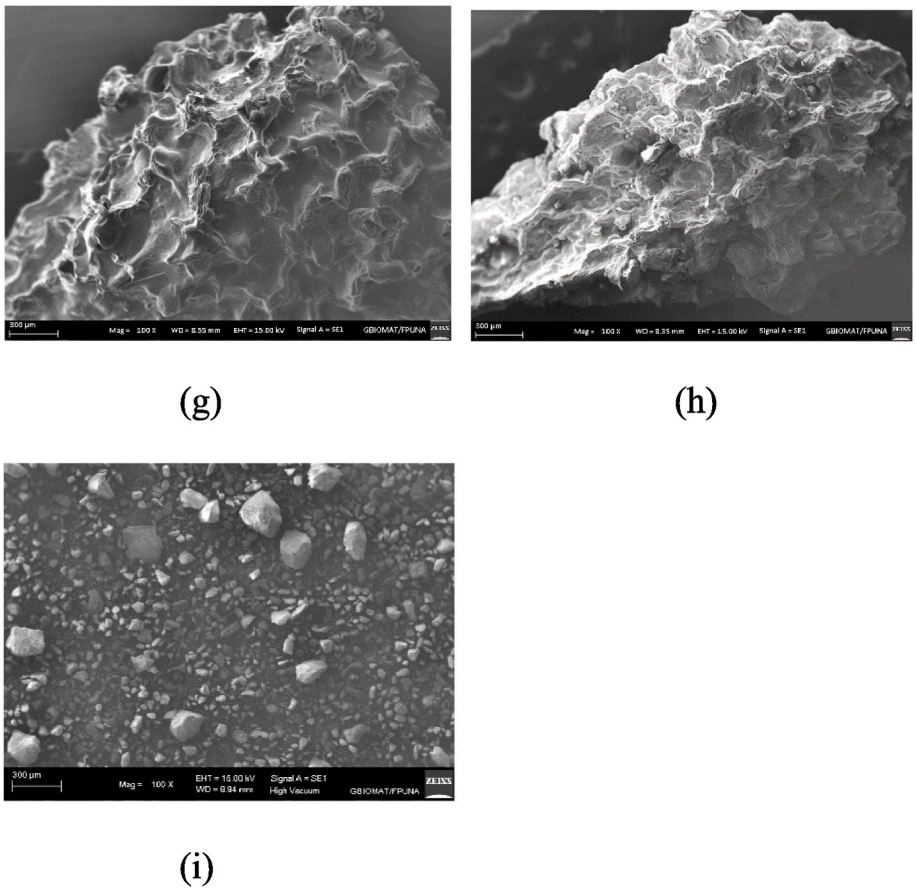

Fig. 4. (*continued*).

porosity of the composite facilitates the entry and movement of lead ions into the internal structure of the adsorbent. According to SEM images in Fig. 4(a–c), it was possible to see air bubbles entrapped and micro-fractures on the biopolymer surface of noodles shape (AA_N), which may indicate high porosity, which improves ion diffusion. Fig. 4 (b, d) shows the hydroxyapatite particles are clearly distinguishable on the surface of the biocomposites (AAH_N); in addition, that could be the reason for slightly higher adsorption kinetics to noodles samples (Fig. 3). However, bead samples presented high unevenness with sharp peaks and deep valleys, which could indicate high roughness (Fig. 4(e–h)). Furthermore, SEM images exhibited stable structure for all samples before and after Pb^{2+} sorption tests.

Likewise, the hydroxyapatite powders used in the present work, which presumably exhibit larger particle sizes (Fig. 4 (i)), showed a sorption capacity of 76.6 mg/g and a corresponding removal efficiency of 76.6 %. However, they required longer time to reach lead saturation. This extended contact time likely reflects a reduced surface area or limited accessibility to sorption sites due to grain growth or particle aggregation.

In contrast, [20]synthesized nano-hydroxyapatite with an average particle size of 83.37 nm via co-precipitation. Their material achieved a significantly higher sorption capacity of 99.31 mg/g and a removal efficiency of 99.2 %, even under high concentration conditions (up to 100 g/mL). Similarly, [21] reported a sorption capacity of 1438.85 mg/g for nanorod-shaped hydroxyapatite. These findings confirm that nanoscale size, enhances the material's interaction with lead ions by increasing the available surface area and active sites.

This behavior can be further explained by the kinetics of the adsorption process. At the initial stage, rapid lead uptake is governed by a physisorption-dominated mechanism, facilitated by the abundance of vacant surface sites. As these sites become progressively occupied, the system shifts towards a slower diffusion-controlled process, where lead ions penetrate into the mesoporous structure of the hydroxyapatite. This transition results in a decline in adsorption rate over time, eventually reaching equilibrium. [21].

Table 2
Remotion efficiency and sorption capacity of the samples AA_B, AA_N, AAH_B and AAH_N.

	AA_B beads	AA_N noodles	AAH_B beads	AAH_N noodles	Hap powder
Remotion efficiency (%)	98.0	98.2	93.3	98.5	76.6
Sorption capacity q_t (mg Pb^{2+}/g of the sample)	98.0	98.2	93.3	98.5	76.6

However, encapsulating hydroxyapatite in the sodium alginate and biological agar prevented its dispersion in the lead solution.

Similar internal structures were expected since the same process parameters were used to produce both formats. However, differences in kinetic parameters were found in the different formats, but the final amount of Pb^{2+} removed was nearly identical across all biocomposites and biopolymers samples.

The amount of Pb^{2+} removed per unit mass of adsorbent and the removal efficiency are presented in Table 2. These values were calculated using equations (1) and (2), respectively. Although the initial heavy metal concentration for the biocomposite AAH_N sample was 1000 ppm and the final concentration was 14.5 ppm, it demonstrated slightly the best performance in terms of removal efficiency. However, pure alginate sorbent beads (AA_B) and noodles samples (AA_N) also performed excellently.

Table 3
Kinetic parameters calculated using pseudo-first and pseudo-second-order models for the adsorption solution of Pb^{2+} ions on the samples.

Samples	Experimental q_e ($mg.g^{-1}$)	Pseudo-first-order			Pseudo-second-order		
		k_1 (min^{-1})	q_e (mgg^{-1})	R^2	k_2 ($g.min^{-1}mg^{2+}_{Pb}$)	q_e ($mg.g^{-1}$)	R^2
AA_B	98.0	0.027	58.34	0.96	$6.48\ x10^{-6}$	111.11	0.99
AAH_B	93.3	0.018	66.52	0.99	$6.23x10^{-4}$	99.24	0.99
AA_N	98.2	0.034	56.23	0.94	$5.71\ x10^{-6}$	101.01	0.99
AAH_N	98.5	0.025	44.67	0.92	$6.17\ x10^{-6}$	101.01	0.99
Hap	76.6	0.013	13.18	0.87	$1.89x10^{-5}$	76.92	0.99

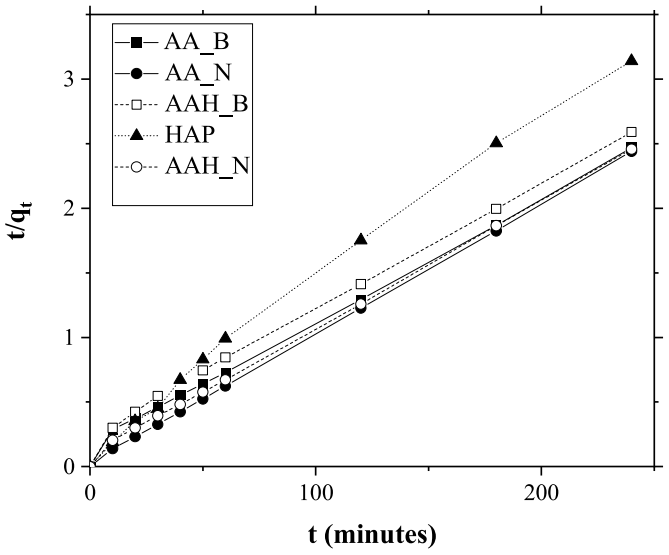

Fig. 5. Data of t/qt versus time according to equation (4) representing the pseudo-second-order kinetics model. Initial Pb^{2+} concentration:1000 mg/L; total contact time: 240 min; agitation speed: 250 rpm; adsorbent dosage: 1.0 g.

3.1. Kinetic studies

In this work, the first- and second-order kinetic models were used to analyze the kinetic behavior based on experimental data from batch experiments. Linear and nonlinear regression equations were applied to determine the best-fitting kinetic model, with the correlation coefficient (R^2) being close to 1 as a criterion. The first- and second-order kinetic models are represented by equations (3) and (4), respectively.

$$Log(q_e - q_t) = \log(q_e) - t^* \frac{k_1}{2.303} \quad (3)$$

$$\frac{t}{q_t} = \frac{1}{k_2 q_e^2} + \frac{1}{q_e} * t \quad (4)$$

In equations (3) and (4), q_t and q_e represent the quantities of lead removed (mg/g sample) from the solution at a specific time and at equilibrium, respectively. The constants k_1 (min^{-1}) and k_2 ($g\ mg^{2+}_{Pb}\ ^{-1}\ min^{-1}$) correspond to the pseudo-first-order and pseudo-second-order rate constants, respectively.

Table 3 shows that the R^2 values are higher for all the samples in the pseudo-second-order kinetics model. The quantity of lead removed (q_e) obtained from the linear plot $\frac{t}{q_t}$ versus t (time), based on the pseudo-second-order rate model given by equation (4), is quite close to the experimental data, as shown in Fig. 5. In contrast, the q_e calculated from the first-order equation did not align with the experimental data. Previous studies reported that the second-order kinetic is more suitable for describing heavy metal uptake by alginate-based materials [1]. Sekar et al. [22] studied the stability enhancement of Hap/SA nanocomposites for effective fluoride adsorption and found with pseudo-second-order kinetics. The modification of sodium alginate with thiosemicarbazide as a new flocculant for heavy metal ions was investigated by [23]. The study showed that the pseudo-second-order model more accurately described the kinetics compared to the pseudo-first-order model [23]. Thus, the pseudo-second-order model suggests that the adsorption process primarily involves chemisorption, that is, lead ions interact with the surfaces of Hap and Hap/SA/Agar.

To better understand the mechanisms of Pb^{2+} removal by the AAH biocomposite developed in this work, SEM and EDX images were analyzed. Figs. 6 and 7 show the results for AA_N, AAH_N, and Hap before Pb^{2+} sorption, and 8 and 9 show the results for AA_N and AAH_N after Pb^{2+} sorption. The literature suggests two mechanisms for Pb^{2+} removal from aqueous solutions by hydroxyapatite ($Ca_{10}(PO_4)_6(OH)_2$) [15]. The first mechanism involves the dissolution of Hap, which produces H_2PO_4 groups due to its high solubility in water. These groups then react with metal ions (M^+) to form a precipitate of $M_{10}(PO_4)_6(OH)_2$ [1]. This mechanism is called dissolution-precipitation and is represented by equations (5) and (6).

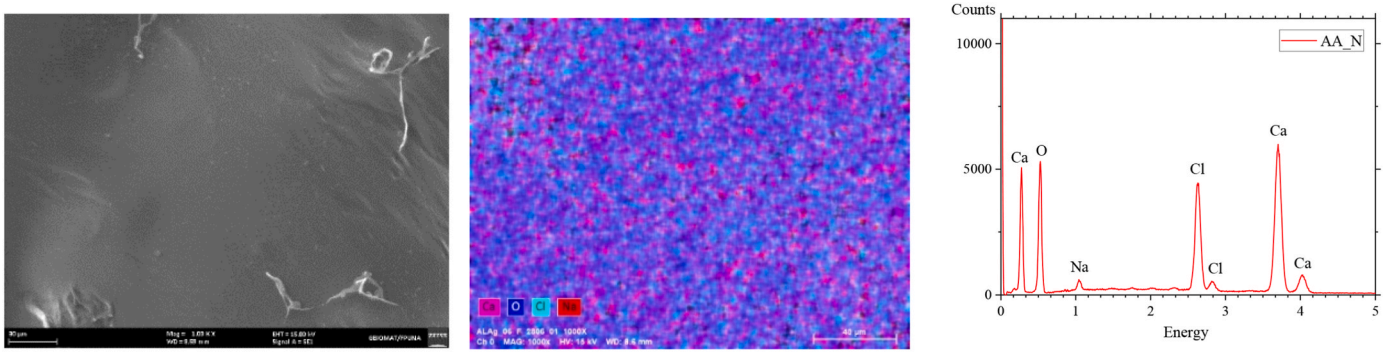

Fig. 6. SEM and EDX images of AA_N sample before Pb^{2+} sorption test. Scale bar: 30 μm, magnification: 100X.

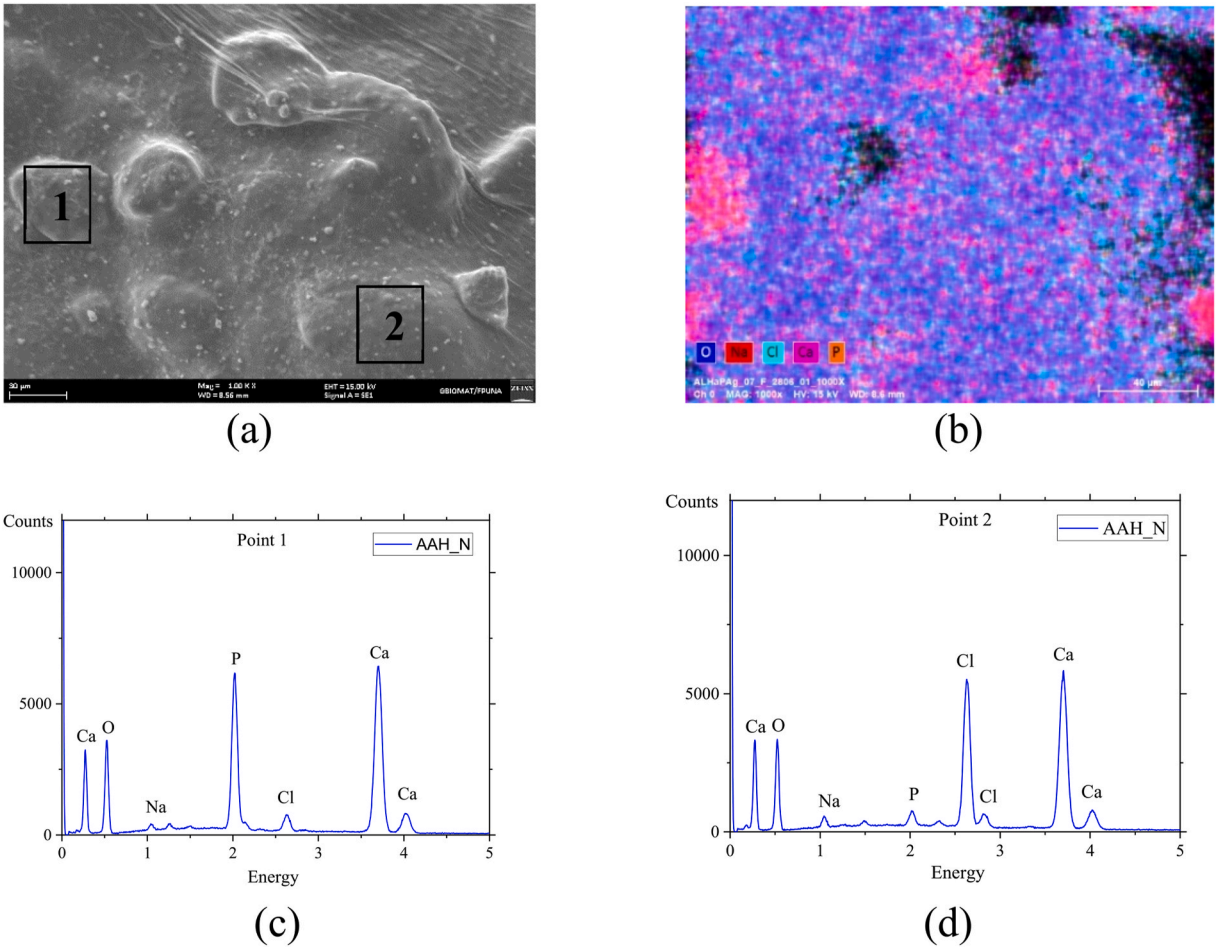

Fig. 7. SEM and EDX images of AAH_N sample before Pb^{2+} sorption test. Scale bar: 30 μm, magnification: 100X.

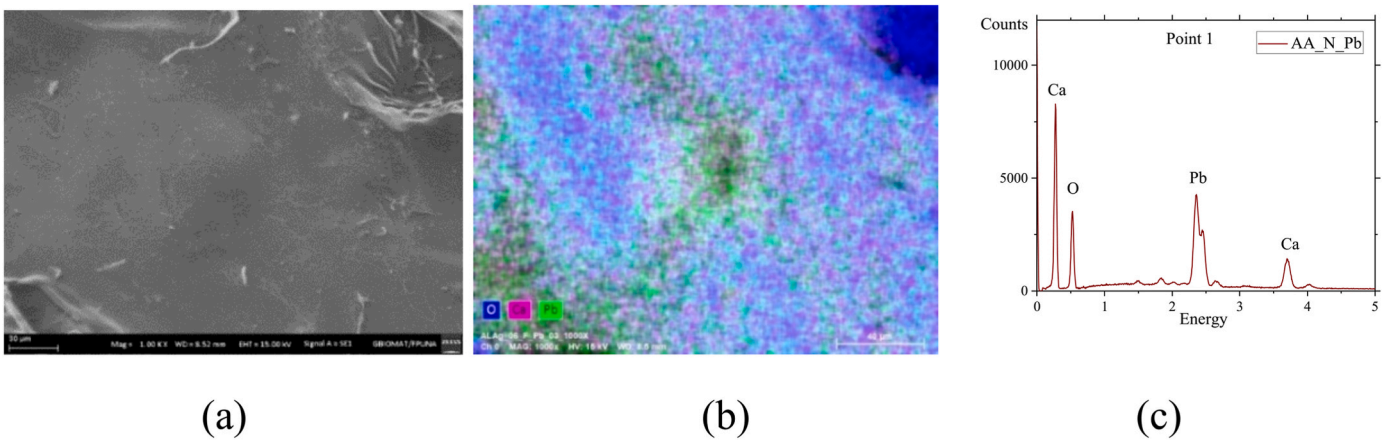

Fig. 8. SEM and EDX images of AA_N sample after Pb^{2+} sorption test. Scale bar: 30 μm, magnification: 100X.

$$\text{Dissolution}: Ca_{10}\,(PO_4)_6(OH)_2 + 14H^+ \rightarrow 10Ca^{2+} + 6H_2\,PO_4^{\ -} + 2H_2O \quad (5)$$

$$\text{Precipitation}: 10Pb^{2+} + 6H_2\,PO_4^{\ -} + 2H_2O \rightarrow 14H^+ + Pb_{10}\,(PO_4)_6(OH)_2 \quad (6)$$

The second mechanism is ion exchange, where Ca^{2+} ions on the surface of Hap are exchanged with Pb^{2+} cations from the solution. This results in the formation of lead apatite compound, $Ca_{(10-x)}\,Pb_x(PO_4)_6(OH)_2$. Additionally, metal complexation may also take place as a secondary mechanism, where oxygen from the functional groups on the surface of the biocomposite forms complexes with the heavy metal ion [24].

SEM images reveal that hydroxyapatite particles, with micrometric size, are present on the surface of the biocomposite (Fig. 7 (a) and 9 (a)). In contrast, the AA_N sample shows a smooth and tight surface (Fig. 6 (a) and 8 (a)), both before and after the adsorption process. The EDX spectra of the AA_N sample before the adsorption process show strong peaks of calcium (Ca), oxygen (O), and chlorine (Cl) and a weak peak of sodium

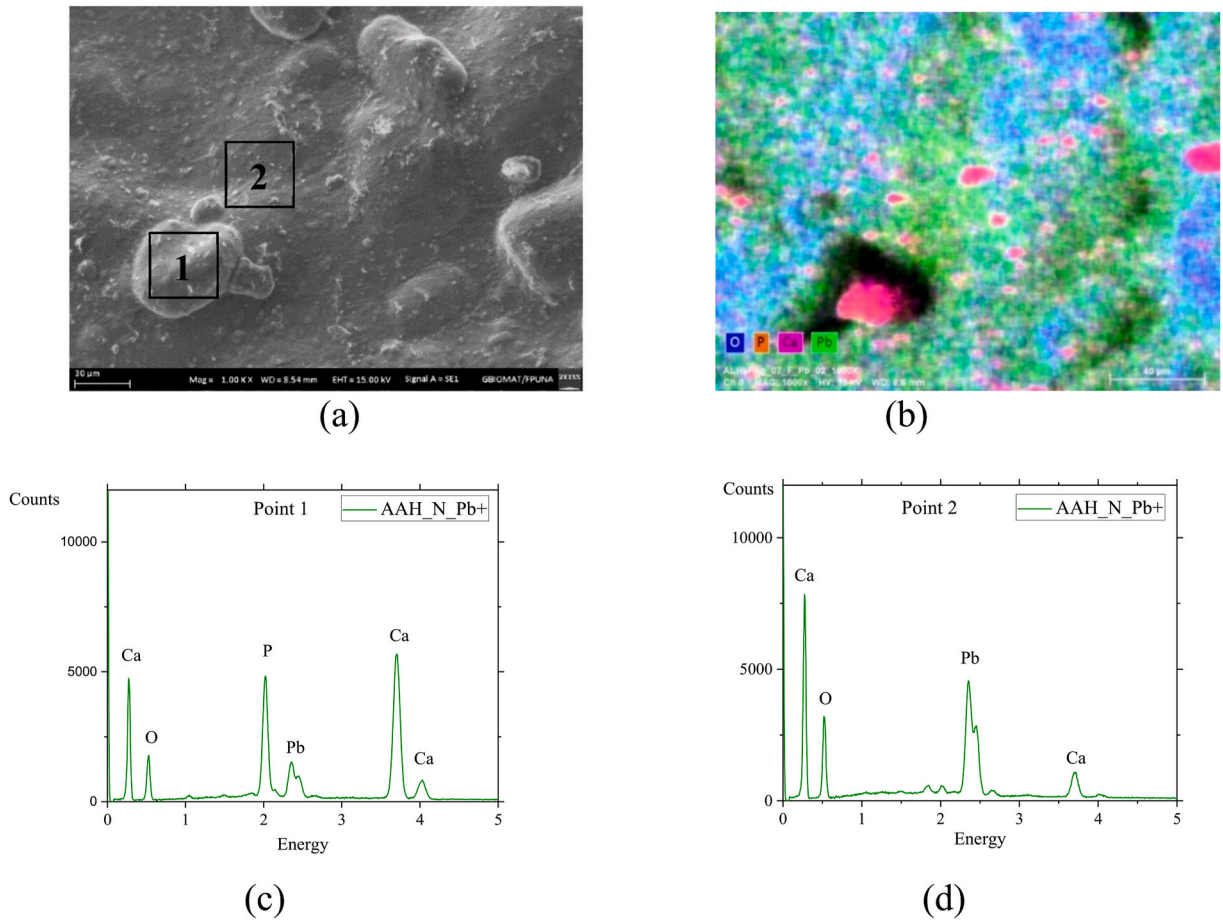

Fig. 9. SEM and EDX images of AAH_N sample after Pb^{2+} sorption test. Scale bar: 30 μm, magnification: 100X.

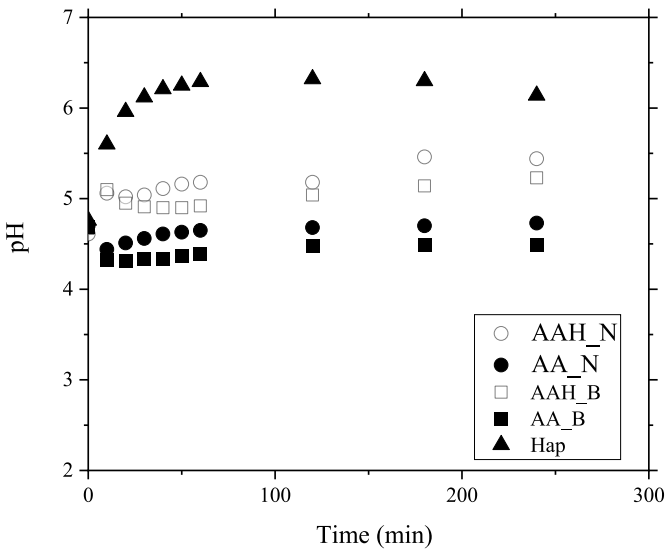

Fig. 10. Variation of lead solution pH versus contact adsorption time for samples AAH_N, AA_N, AAH_B, AA_B. Initial Pb^{2+} concentration:1000 mg/L; total contact time: 240 min; agitation speed: 250 rpm; adsorbent dosage: 1.0 g.

(Na) (Fig. 6 (c)). The chlorine peak came from the $CaCl_2$ solution of the gelation mechanism [15]. The spectra of the AAH_N biocomposite sample shows that point 1 primarily consists of hydroxyapatite components, specifically phosphorous (P) and calcium (Ca). At point 2, strong chlorium (Cl) and calcium (Ca) peaks are observed, as well as weak peaks of phosphorous (P) and sodium (Na). After Pb^{2+} sorption, the EDX images of AAH_N and AA_N samples revealed the elemental composition of the biocomposite, including phosphorous (P), and calcium (Ca) from hydroxyapatite at point 1, and oxygen (O) from sodium alginate and agar at point 2. Besides, the presence of a lead (Pb^{2+}) peak at point 2 (Fig. 9(c) and (d)) was confirmed by elemental mapping, which showed because most of the lead was distributed on the surface of sodium alginate and agar components (Fig. 8 (b)). Meanwhile, the hydroxyapatite surface shows mainly calcium (Fig. 9 (b)). These results suggest that one on the adsorption mechanisms in hydroxyapatite is likely dissolution–precipitation, as indicated by the presence of unchanged peaks of phosphorus (P), calcium (Ca), and lead (Pb^{2+}) at point 1. In addition, when the adsorption occurred in the biopolymer surfaces in both samples (AA_N and AAH_N), a reduction in the remaining peaks for oxygen and calcium were observed (Fig. 8 (c) and 9 (d)). This suggests that the predominant adsorption mechanism in biopolymer area of the samples AA_N and AAH_N is likely ion exchange.

Sutirman et al. [1] and Zhang et al. [25] identified solution pH as a critical parameter influencing the adsorption rate, ionization degree, metal speciation, and surface charge of the adsorbent. In this work, all the solutions for the adsorption process started with an initial pH of around 4.7 (Fig. 10). Biopolymer-based sorbents typically pH work effectively within a pH range of 4–6 [1]. The efficiency of Pb^{2+} ion removal by hydroxyapatite is highly influenced by an initial pH between 4 and 5 [20]. Besides, alginate/agar adsorbents are known to contain numerous carboxyl groups (-COOH) in their composition. In this sense, carboxyl groups tend to ionize, increasing the concentration of H^+ protons, which lowers the pH [26,27]. Fig. 10 shows a decrease in pH within 10 min for alginate/agar sorbent samples (AA_N, AA_B) when in contact with the lead solution. This indicates that the ionized carboxyl

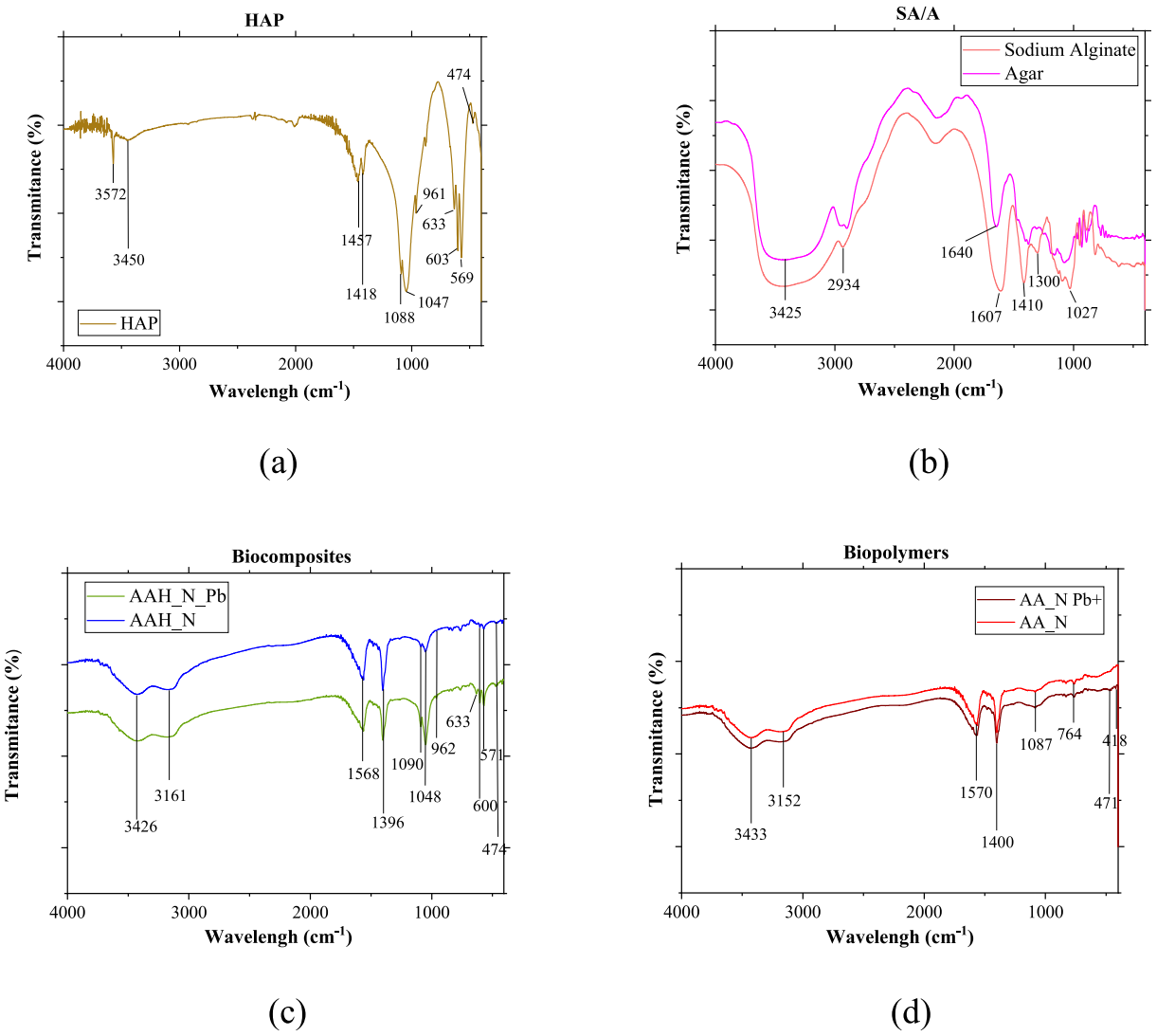

Fig. 11. FTIR spectrum of (a) pure hydroxyapatite, (b) pure sodium alginate and agar, (c) biocomposites AAH_N and AAH_N with Pb^{2+}, and (d) and biopolymers AA_N and AA_N with Pb^{2+}.

groups become available to capture the Pb^{2+} cations. However, the pH for AA_N slightly increased during the adsorption, which suggests the possibility of ions exchange between Pb^{2+} and Ca^{2+} cations, leading to the formation of a stable structure.

Nevertheless, the behavior of the biocomposites AAH_N and AAH_B in the lead solution showed a slight increase in pH. This can be attributed to the presence of Ca^{2+} cations from hydroxyapatite and the 'egg box' structure of the biopolymer. According to equation (5),

Table 4
FTIR spectral ranges and corresponding functional groups identified in this study.

Bands of this work	Functional Group	This work HAP	This work SA/A	This work Biocomposites	This work Biopolymers	References
3360	O–H stretching	3450	3425	3426	3436	[28]
2926	C–H_2 asymmetric and symmetric stretching of methylene	–	2934	3161	3152	[31]
1640	C═O amide I group	—	1640	–	–	[31–33]
1640	O–H					[29,30]
1625	asymmetric stretching vibration of COO^- of alginate	—	1607	1568	1570	[28]
1460 and 1530	CO_3^{2-} group of HAP	1457	–	–	–	[34]
1417	symmetrical stretching modes of COO^-	1418	1418	1396	1400	[28]
1033–1097	PO_4^{3-} asymmetry bending υ_3 of Hap and C–O–C of sodium alginate	1047	–	1048	—	[30] [18,35, 36].
962	Symmetric P–O stretching (υ_1) of Hap	961	962	–		[30]
630	Weak peak of O–H	633	–	633	–	[18,34]
560 and 600	PO_4^{3-} bending υ_4	569/603	–	571/633	–	[18,34]
471	PO_4^{3-} streching υ_2	474	–	474	–	[18,29,34]

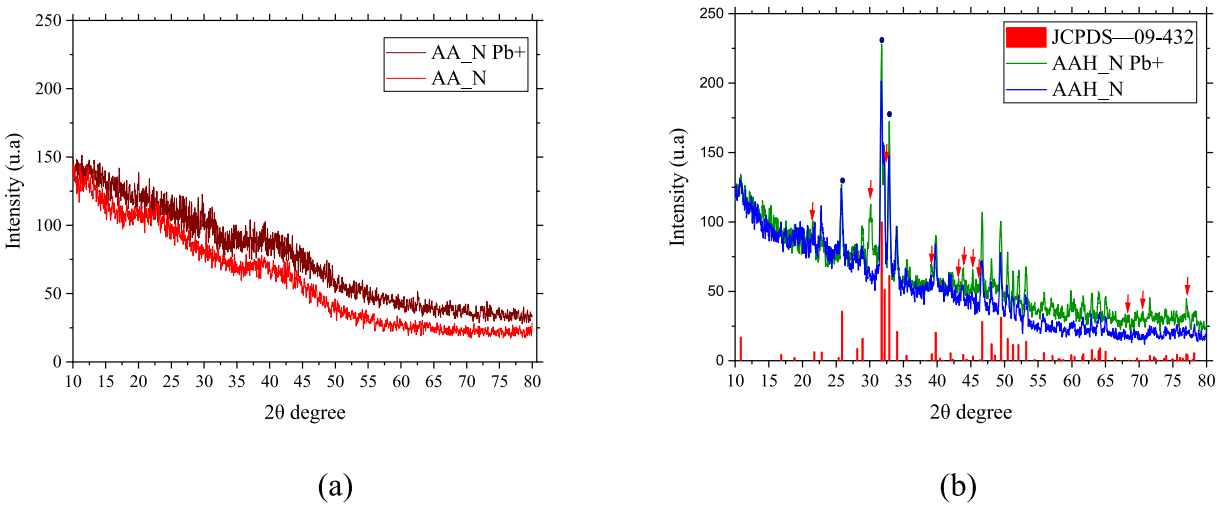

Fig. 12. X-ray diffraction patterns for AA_N, AA_N Pb^{2+} (biopolymers) (a) and AAH_N, AAH_N Pb^{2+} (biocomposites) (b).

hydroxyapatite produces H_2PO_4 groups, leading to the formation of the compound $Pb_{10}\ (PO_4)_6(OH)_2$ described in equation (6). Additionally, another mechanism that may occur is ion exchange, where Ca^{2+} ions on the surface of pure hydroxyapatite and the biocomposites are exchanged with Pb^{2+} cations from the solution. This results in the formation of the lead apatite compound $Ca_{(10-x)}\ Pb_x(PO_4)_6(OH)_2$.

The FTIR spectrum (Fig. 11) shows the functional groups of AAH_N, AA_N samples (Fig. 11c and d), pure hydroxyapatite (Fig. 11a) and pure sodium alginate and biological agar (Fig. 11b). The band at 3360 and 1640 cm^{-1} was assigned to the O–H stretching of sodium alginate [28–30]. The absorption band at 2926 cm^{-1}, corresponding to the symmetric and asymmetric stretching of methylene (-CH_2), is characteristic of pure biopolymers [31]. The band at 1640 cm^{-1} corresponds to the stretching of a conjugated peptide bond by an amine (NH) and acetone group (CO) [31–33] from the biopolymers. The two absorption peaks at 1625 cm^{-1} and 1417 cm^{-1} are attributed to the asymmetric and symmetrical stretching modes of COO^- [28]. Two characteristic peaks from hydroxyapatite, observed between 1460 cm^{-1} and 1530 cm^{-1} are attributed to carbonate groups [34]. The adsorption bands observed around 962 cm^{-1}, 471 cm^{-1}, 1033 cm^{-1} – 1097 cm^{-1}, 560 cm^{-1} – 600 cm^{-1} correspond to υ_1, υ_2, υ_3, and υ_4 vibrational modes of the phosphate group from hydroxyapatite, respectively [18,35,36], [29, 30]. A weak O–H peak can also be observed at 630 cm^{-1} [18,34]. Table 4 shows the characteristic features of each FTIR spectral range and the corresponding functional groups identified in this study.

According to Rajkumar et al. [29], the weak peak around 962 cm^{-1} associated with the phosphate group bands υ_1 from hydroxyapatite decreased in intensity due to the presence of sodium alginate and agar, which is attributed to the blocking of active sites of the biopolymers. Zhou et al. [30] mentioned a slight shift around 1640 cm^{-1} due to the formation of H_2PO_4 groups, leading to the generation of $Pb_{10}\ (PO_4)_6(OH)_2$ based on a dissolution-precipitation mechanism. Furthermore, the FTIR spectra of the biocomposites and biopolymers samples show a displacement related to the pure components, a behavior attributed to the strong interaction between OH, COO^- and NHR groups [37].

To study the structural changes in the biofilters and determine their degree of crystallinity, X-ray diffraction (XRD) was performed before and after the sorption process. Fig. 12 shows the XRD pattern of AAN, AA_N Pb^{2+} (biopolymers), and AAH_N, AAH_N Pb^{2+} (biocomposites). XRD pattern of biopolymers AAN and AA_N Pb^{2+} exhibit an amorphous structure, as shown in Fig. 12 (a)) [36]. In contrast, Fig. 12 (b) shows the XRD pattern of AAH_N sample before the sorption process, which reveals characteristic intense peaks at 2θ values of 25.77, 31.73, 32.91, which are attributed to hexagonal hydroxyapatite structure, indicating crystallinity according to the pattern of pure Hap (JC PDS 09–432). Additionally, Fig. 12 (b) displays the diffraction pattern of AAH_N Pb^{2+} after sorption process. The pattern reveals two distinct phases: the hydroxyapatite phase and a new hydroxy pyromorphite phase $(Pb_{10}\ (PO_4)_6(OH)_2)$. The hydroxy pyromorphite is characterized by an intense peak at 30.13° [38]. Other smaller peaks at 21.51, 32.11, 39.13, 43.19, 43.83, 45.81, 47.15, 68.23, 70.51, and 77.05° are also present, which are attributed to the same material [30]. The formation of lead phosphate, such as hydroxy pyromorphite, confirms that the main lead sorption mechanism on the hydroxyapatite surface was dissolution-precipitation [38].

4. Conclusions

The sodium alginate/hydroxyapatite/agar biocomposites were successfully produced in two formats: noodles and beads, both with and without hydroxyapatite. These biocomposites were evaluated as filters for Pb^{2+} removal from aqueous solutions. Adsorption experiments demonstrated that the efficiency of Pb^{2+} ion removal was approximately 98.5 % for the noodle format, while all biofilters exhibited high efficiency. The data were well-aligned with the pseudo-second-order kinetics model. Thus, the results indicate that regardless of the format – noodles or beads - both types of adsorbent materials can be effectively used for environmentally friendly removal of heavy metals from wastewater. However, the adsorption kinetics process was faster for the noodle samples compared to the beads. Furthermore, the biocomposite materials aid in encapsulating powdered hydroxyapatite, preventing its dispersion in aqueous solution.

CRediT authorship contribution statement

Maria M. Espinola Colmán: Writing – review & editing, Writing – original draft, Validation, Methodology, Investigation, Funding acquisition, Formal analysis, Data curation, Conceptualization. **Lucas Medina:** Methodology. **Pablo Casanova:** Validation, Methodology. **Maria B. Martinez P:** Writing – review & editing. **Magna Monteiro:** Writing – review & editing, Supervision, Resources.

Declaration of competing interest

The authors declare that they have no known competing financial interests or personal relationships that could have appeared to influence the work reported in this paper.

Acknowledgments

The authors are grateful to CONACYT/PROCIENCIA/FEEI/Paraguay for the financial support through the PIRT 19-3 and PRIE 19–21 programs.

Data availability

The research data are available in the article

References

[1] Sutirman, Z.A., Sanagi, M.M., Wan Aini, W.I., 2021. Alginate-based adsorbents for removal of metal ions and radionuclides from aqueous solutions: a review. Int. J. Biol. Macromol. 174, 216–228. https://doi.org/10.1016/j.ijbiomac.2021.01.150. Elsevier B.V.

[2] Burakov, A.E., Galunin, E.V., Burakova, I.V., Kucherova, A.E., Agarwal, S., Tkachev, A.G., Gupta, V.K., 2018. Adsorption of heavy metals on conventional and nanostructured materials for wastewater treatment purposes: a review. Ecotoxicol. Environ. Saf. 148, 702–712. https://doi.org/10.1016/j.ecoenv.2017.11.034. Academic Press.

[3] Riva, M.A., Lafranconi, A., D'Orso, M.I., Cesana, G., 2012. Lead poisoning: historical aspects of a paradigmatic "occupational and environmental disease.". Saf. Health Work 3 (1), 11–16. https://doi.org/10.5491/SHAW.2012.3.1.11. Elsevier Science B.V.

[4] Prüss-Üstün, Annette, Mathers, Colin, Corvalán, Carlos, Woodward, Alistair, 2003. Assessing the Environmental Burden of Disease at National and Local Levels : Introduction and Methods. World Health Organization.

[5] Abdullah, N., Yusof, N., Lau, W.J., Jaafar, J., Ismail, A.F., 2019. Recent trends of heavy metal removal from water/wastewater by membrane technologies. J. Ind. Eng. Chem. 76, 17–38. https://doi.org/10.1016/j.jiec.2019.03.029. Korean Society of Industrial Engineering Chemistry.

[6] Park, H.G., Kim, T.W., Chae, M.Y., Yoo, I.K., 2007. Activated carbon-containing alginate adsorbent for the simultaneous removal of heavy metals and toxic organics. Process Biochem. 42 (10), 1371–1377. https://doi.org/10.1016/j.procbio.2007.06.016.

[7] Kong, C., Zhao, X., Li, Y., Yang, S., Chen, Y.M., Yang, Z., 2020. Ion-induced synthesis of alginate fibroid hydrogel for heavy metal ions removal. Front. Chem. 7. https://doi.org/10.3389/fchem.2019.00905.

[8] Elwakeel, K.Z., Ahmed, M.M., Akhdhar, A., Sulaiman, M.G.M., Khan, Z.A., 2022. Recent advances in alginate-based adsorbents for heavy metal retention from water: a review. Desalination Water Treat. 272, 50–74. https://doi.org/10.5004/dwt.2022.28834.

[9] Suzuki, T., Hatsushika, T., Yasumasa, H., 1981. Synthetic hydroxyapatites employed as inorganic cation-exchangers. J. Chem. Soc. Faraday Trans. I 77.

[10] Reichert, J., Binner, J.G.P., 1996. An evaluation of hydroxyapatite-based filters for removal of heavy metal ions from aqueous solutions. J. Mater. Sci. 31.

[11] Balasooriya, I.L., Chen, J., Gedara, S.M.K., Han, Y., Wickramaratne, M.N., 2022. Applications of nano hydroxyapatite as adsorbents: a review. Nanomaterials 12 (14). https://doi.org/10.3390/nano12142324. MDPI.

[12] Wang, J., Chen, C., 2009. Biosorbents for heavy metals removal and their future. Biotechnol. Adv. 27 (2), 195–226. https://doi.org/10.1016/j.biotechadv.2008.11.002.

[13] Wang, B., Wan, Y., Zheng, Y., Lee, X., Liu, T., Yu, Z., Huang, J., Ok, Y.S., Chen, J., Gao, B., 2019. Alginate-based composites for environmental applications: a critical review. Crit. Rev. Environ. Sci. Technol. 49 (4), 318–356. https://doi.org/10.1080/10643389.2018.1547621.

[14] Callister, W.D.J., Rethwisch, D.G., 2018. Materials Science and Engineering: an Introduction (Tenth). Wiley.

[15] Googerdchian, F., Moheb, A., Emadi, R., 2012. Lead sorption properties of nanohydroxyapatite-alginate composite adsorbents. Chem. Eng. J. 200–202, 471–479. https://doi.org/10.1016/j.cej.2012.06.084.

[16] Yang, X., Zhou, T., Ren, B., Hursthouse, A., Zhang, Y., 2018. Removal of Mn (II) by sodium alginate/graphene oxide composite double-network hydrogel beads from aqueous solutions. Sci. Rep. 8 (1). https://doi.org/10.1038/s41598-018-29133-y.

[17] Sangeetha, K., Vidhya, G., Vasugi, G., Girija, G.V.E.K., 2018. Lead and cadmium removal from single and binary metal ion solution by novel hydroxyapatite/alginate/gelatin nanocomposites. J. Environ. Chem. Eng. 6 (1), 1118–1126. https://doi.org/10.1016/j.jece.2018.01.018.

[18] Caballero, N., Ozuna, P.C., Monteiro, M., 2019. Kinetic analysis of lead removal by natural hydroxyapatite from aqueous solution in high concentration. Mater. Res. 22. https://doi.org/10.1590/1980-5373-MR-2018-0859.

[19] Dogan, H., 2012. Preparation and characterization of calcium alginate-based composite adsorbents for the removal of Cd, Hg, and Pb ions from aqueous solution. Toxicol. Environ. Chem. 94 (3), 482–499. https://doi.org/10.1080/02772248.2012.659249.

[20] Iconaru, S.L., Motelica-Heino, M., Guegan, R., Beuran, M., Costescu, A., Predoi, D., 2018. Adsorption of Pb (II) ions onto hydroxyapatite nanopowders in aqueous solutions. Materials 11 (11). https://doi.org/10.3390/ma11112204.

[21] Jiang, J., Long, Y., Hu, X., Hu, J., Zhu, M., Zhou, S., 2020. A facile microwave-assisted synthesis of mesoporous hydroxyapatite as an efficient adsorbent for Pb2+ adsorption. J. Solid State Chem. 289. https://doi.org/10.1016/j.jssc.2020.121491.

[22] Sekar, S., Panchu, S.E., Kolanthai, E., Rajaram, V., Subbaraya, N.K., 2022. Enhanced stability of hydroxyapatite/sodium alginate nanocomposite for effective fluoride adsorption. Mater. Today Proc. 58, 909–917. https://doi.org/10.1016/j.matpr.2021.12.064.

[23] Tian, Z., Zhang, L., Shi, G., Sang, X., Ni, C., 2018. The synthesis of modified alginate flocculants and their properties for removing heavy metal ions of wastewater. J. Appl. Polym. Sci. 135 (31). https://doi.org/10.1002/app.46577.

[24] Nie, J., Dan, Z., Yaoyu, Z., 2021. Magnetic biochar-based composites for removal of recalcitrant pollutants in water. In: Sorbents Materials for Controlling Environmental Pollution: Current State and Trends. Elsevier, pp. 163–187. https://doi.org/10.1016/B978-0-12-820042-1.00015-8.

[25] Zhang, L., Zeng, Y., Cheng, Z., 2016. Removal of heavy metal ions using chitosan and modified chitosan: a review. J. Mol. Liq. 214, 175–191. https://doi.org/10.1016/j.molliq.2015.12.013. Elsevier.

[26] Wanga, Xiaohuan, Zheng, Yian, Wanga, Aiqin, 2009. Fast removal of copper ions from aqueous solution by chitosan-g-poly(acrylic acid)/attapulgite composites. J. Hazard Mater. 168, 970–977.

[27] Gao, L., Li, Z., Yi, W., Wang, L., Song, N., Zhang, W., Li, G., Wang, S., Li, N., Zhang, A., 2023. Effective Pb2+adsorption by calcium alginate/modified cotton stalk biochar aerogel spheres: with application in actual wastewater. J. Environ. Chem. Eng. 11 (1). https://doi.org/10.1016/j.jece.2022.109074.

[28] Guo, T., Pei, Y., Tang, K., He, X., Huang, J., Wang, F., 2017. Mechanical and drug release properties of alginate beads reinforced with cellulose. J. Appl. Polym. Sci. 134 (8). https://doi.org/10.1002/app.44495.

[29] Rajkumar, M., Meenakshisundaram, N., Rajendran, V., 2011. Development of nanocomposites based on hydroxyapatite/sodium alginate: synthesis and characterisation. Mater. Char. 62 (5), 469–479. https://doi.org/10.1016/j.matchar.2011.02.008.

[30] Zhou, C., Wang, X., Wang, Y., Song, X., Fang, D., Ge, S., 2021. The sorption of single- and multi-heavy metals in aqueous solution using enhanced nano-hydroxyapatite assisted with ultrasonic. J. Environ. Chem. Eng. 9 (3). https://doi.org/10.1016/j.jece.2021.105240.

[31] Yin, Z.C., Wang, Y.L., Wang, K., 2018. A pH-responsive composite hydrogel beads based on agar and alginate for oral drug delivery. J. Drug Deliv. Sci. Technol. 43, 12–18. https://doi.org/10.1016/j.jddst.2017.09.009.

[32] Guerrero, P., Etxabide, A., Leceta, I., Peñalba, M., De La Caba, K., 2014. Extraction of agar from Gelidium sesquipedale (Rodhopyta) and surface characterization of agar based films. Carbohydr. Polym. 99, 491–498. https://doi.org/10.1016/j.carbpol.2013.08.049.

[33] Sharma, K., Kumar, V., Swart-Pistor, C., Chaudhary, B., Swart, H.C., 2017. Synthesis, characterization, and anti-microbial activity of superabsorbents based on agar-poly(methacrylic acid-glycine). J. Bioact. Compat Polym. 32 (1), 74–91. https://doi.org/10.1177/0883911516653148.

[34] Gheisari, H., Karamian, E., Abdellahi, M., 2015. A novel hydroxyapatite -Hardystonite nanocomposite ceramic. Ceram. Int. 41 (4), 5967–5975. https://doi.org/10.1016/j.ceramint.2015.01.033.

[35] Grouli, A., Bachra, Y., Damiri, F., Pandit, V.U., Berrada, M., 2023. Removal of pollutants from wastewater using Fe-doped hydroxyapatite encapsulated with alginate. Biointerface Res. Appl. Chem. 13 (5). https://doi.org/10.33263/BRIAC135.438.

[36] Sangeetha, K., Thamizhavel, A., Girija, E.K., 2013. Effect of gelatin on the in situ formation of Alginate/Hydroxyapatite nanocomposite. Mater. Lett. 91, 27–30. https://doi.org/10.1016/j.matlet.2012.09.054.

[37] Mao, X., Wang, L., Gu, S., Duan, Y., Zhu, Y., Wang, C., Lichtfouse, E., 2018. Synthesis of a three-dimensional network sodium alginate–poly(acrylic acid)/attapulgite hydrogel with good mechanic property and reusability for efficient adsorption of Cu2+ and Pb2+. Environ. Chem. Lett. 16 (2), 653–658. https://doi.org/10.1007/s10311-018-0708-9.

[38] Mavropoulos, E., Rocha-Leão, M.H., da Rocha, N.C.C., Prado da Silva, M.H., Rossi, A.M., 2007. Hydroxyapatite-alginate composite for lead removal in artificial gastric fluid. J. Mater. Res. 22 (12), 3371–3377. https://doi.org/10.1557/jmr.2007.0419.